

THE COMPOSITION OF ZIRCON IN THE PERALUMINOUS HERCYNIAN GRANITES OF THE SPANISH CENTRAL SYSTEM BATHOLITH

CECILIA PÉREZ-SOBA[§], CARLOS VILLASECA AND JOSÉ GONZÁLEZ DEL TÁNAGO

*Departamento de Petrología y Geoquímica, Facultad de Ciencias Geológicas,
 Universidad Complutense, E-28040 Madrid, Spain*

LUTZ NASDALA

Institut für Mineralogie und Kristallographie, Universität Wien, A-1090 Wien, Austria

ABSTRACT

We have investigated the zircon from granites of the Spanish Central System (SCS) batholith. This batholith is composed of plutons of both I- and S-type granite, with different degrees of fractionation. The association provides a natural laboratory for the study of compositional evolution of zircon. We recognize two types of magmatic zircon. Type-1 zircon consists of euhedral and elongate crystals showing an oscillatory zoning, usually hosted in the early major minerals, being more abundant in granodiorite and monzogranite plutons. Type-2 zircon is characterized by smaller and more equant crystals, unzoned, or irregularly zoned, and usually interstitial to the rock-forming minerals, and forming clusters with other accessory minerals. This second type is more abundant in leucogranites, aplites and pegmatites. Type-2 zircon shows the highest concentrations of Hf (16.58 wt.% HfO₂), U (4.83% UO₂), Th (4.87% ThO₂), Y (8.51% Y₂O₃), and HREE (3.78% HREE₂O₃), and the lowest analytical totals (down to 91.2%). The replacement of Zr by tetravalent cations (Th, U and Hf) is favored in the most evolved granites. Micro-areas of zircon with low analytical totals (91–98 wt.%) have a high level of cation substitution. Moreover, their high Th–U contents induce elevated levels of radiation damage. Disturbances in the original structure, combined with severe metamictization of U–Th-rich micro-areas, may have caused an enhanced susceptibility to secondary alteration. This process, in turn, is believed to have formed the observed strongly damaged and cation-deficient zircon. The range of Zr/Hf values in zircon crystals of the granites studied and those of related metamorphic rocks (as possible crustal sources) are similar. The composition of zircon from SCS granulite xenoliths overlaps with the compositional field of zircon from granite, supporting previous models of crustal recycling for the origin of the SCS batholith.

Keywords: zircon, composition, trace elements, I-type granite, S-type granite, peraluminous granulites, Iberian Hercynian Belt, Spanish Central System.

SOMMAIRE

Nous avons étudié le zircon provenant des granites du batholite du Système Central Espagnol. Ce batholite comprend des plutons de type I aussi bien que de type S, avec des degrés de fractionnement variables. L'association fournit un excellent laboratoire naturel pour l'étude de l'évolution compositionnel du zircon, qui peut avoir un de deux aspects. Le zircon de type 1 se présente en cristaux idiomorphes et allongés montrant une zonation oscillatoire, généralement englobés dans les minéraux majeurs précoces; il est donc plutôt abondant dans les plutons granodioritiques et monzonitiques. Le zircon de type 2 se présente en cristaux plus petits et plus équidimensionnels, non zonés ou bien zonés de façon irrégulière, et généralement tardifs, en position interstitielle parmi les minéraux majeurs de la roche, et regroupés avec d'autres minéraux accessoires. Le zircon de type 2 est plus abondant dans les leucogranites, aplites et pegmatites. Il montre les teneurs les plus élevées en Hf (16.58 wt.% HfO₂), U (4.83% UO₂), Th (4.87% ThO₂), Y (8.51% Y₂O₃), et terres rares lourdes (3.78% des oxydes), et les totaux d'analyses les plus faibles (jusqu'à 91.2%, poids). Le remplacement du Zr par les cations tétravalents Th, U et Hf serait favorisé dans les granites les plus évolués. Les micro-régions du zircon ayant un faible total analytique (91–98%) possèdent un niveau élevé de remplacement par ces cations. De plus, leurs teneurs élevées en Th et U ont produit un niveau élevé de dommage dû à la radiation. Les distorsions causées à la structure du zircon, en plus de la métamictisation avancée des micro-régions les plus riches en U et Th, pourraient avoir causé la susceptibilité accrue du zircon de type 2 à l'altération secondaire, qui rendrait compte des compositions fortement déficitaires du zircon endommagé. Les valeurs du rapport Zr/Hf des cristaux de zircon dans les granites étudiés et dans les roches métamorphiques apparentées (comme sources possibles dans la croûte) sont semblables. La composition du zircon

[§] E-mail address: pesoa@geo.ucm.es

dans les enclaves granulitiques de ce batholite chevauche celle du zircon des granites, étayant les modèles d'un recyclage des roches de la croûte pour expliquer celles du batholite.

(Traduit par la Rédaction)

Most-clés: zircon, composition, éléments traces, granite de type I, granite de type S, granulites hyperalumineuses, Ceinture Hercynienne Ibérique, batholite du Système Central Espagnol.

INTRODUCTION

Zircon is one of the most widespread accessory mineral in granites, and particularly in peraluminous granites and granulitic metamorphic rocks (Wark & Miller 1993, Bea 1996, Villaseca *et al.* 2003). It is characterized by its high durability to weathering, alteration, metamorphism and resistance to high-temperature diffusive re-equilibration (*e.g.*, Watson 1996). Favored by these unique properties, zircon has received considerable attention in the past decades as a thermochronological indicator (*e.g.*, Hanchar & Hoskin 2003, and references therein) and for its potential application as a host material for the safe storage of nuclear waste (*e.g.*, Mathieu *et al.* 2001, Ewing *et al.* 2003). Zircon is used as a crude thermometer for crystallization conditions and as petrogenetic indicator (*e.g.*, Pupin 1980, Harrison & Watson 1983, Vavra 1994, Hanchar & Watson 2003, Valley 2003, Kempe *et al.* 2004, Watson *et al.* 2006). Moreover, zircon is widely used in geochronological studies (*e.g.*, Mezger & Krogstad 1997, Solar *et al.* 1998, Parrish & Noble 2003, Hanchar & Hoskin 2003, Jackson *et al.* 2004).

The composition of zircon varies widely owing to solid solution with xenotime (Y, HREE), and the substitution $Zr_{-1}(Hf,Th,U)_1$. Many studies have been devoted to zircon composition in a wide variety of rocks (*e.g.*, Pupin 2000, Caironi *et al.* 2000, Rubatto *et al.* 2001, Hoskin & Schaltegger 2003, Fedo *et al.* 2003, Belousova *et al.* 2002, 2006). Indeed, trace-element contents and elemental ratios have been suggested both as indicator of magma fractionation (*e.g.*, Černý *et al.* 1985, Irber *et al.* 1997, Uher & Černý 1998, Wang *et al.* 2000, Koreneva & Zaráisky 2004, Breiter *et al.* 2006), and as a crude estimate of magma source (*e.g.*, Uher *et al.* 1998, Hoskin & Ireland 2000, Pupin 1992, 2000, Belousova *et al.* 2006, Lowery *et al.* 2006). Some trace elements (Hf, Th, U, Y, HREE) attain a very high concentration in zircon from some felsic products of fractionation (Wang *et al.* 1996, Heaman *et al.* 1990, Hoskin & Schaltegger 2003) and especially in some pegmatites (*e.g.*, Wang *et al.* 1996, Uher & Černý 1998, Seidler *et al.* 2005).

In this paper, we study the composition of zircon from a group of Hercynian plutons of the Spanish Central System (SCS) batholith, comprising S- and I-type granites with variable degrees of fractionation (Villaseca *et al.* 1998, Villaseca & Herreros 2000). We also compare the geochemical features of zircon in

granite with those of zircon from lower-crust granulitic xenoliths, the presumed residual counterpart of the granitic SCS batholith (Villaseca *et al.* 1999).

DESCRIPTION OF THE GRANITIC PLUTONS OF THE SPANISH CENTRAL SYSTEM

The SCS batholith, located in central Spain, extends over an area of about 10,000 km². It was emplaced during the late stages of the Hercynian orogeny, mainly from 325 to 285 Ma (Villaseca & Herreros 2000). The SCS batholith is almost entirely composed of peraluminous granitic rocks. Three types of granite have been distinguished on the basis of their degree of peraluminosity: i) moderately peraluminous cordierite-bearing granites of S-type affinity, ii) weakly peraluminous to metaluminous granitic rocks with locally accessory amphibole and affinity with I-type granites, and iii) transitional types of biotite-bearing granitic rocks of intermediate peraluminous character (Villaseca *et al.* 1998). Five plutons representative of this I- and S-type variability has been selected for this study focused on zircon. The mineralogical data gathered on these granitic plutons are summarized in Table 1.

Of the five plutons, three are of I-type composition (Fig. 1). The Atalaya Real pluton is a small circular massif (18 km²) showing a wide lithological range. It is mainly composed of equigranular coarse-grained amphibole and biotite-bearing granitic rocks ranging from granodiorite to monzogranite. In the outermost margin, a leucogranitic facies with associated aplitic bodies is locally developed. A Rb–Sr isochron age of 284 ± 13 Ma was reported for this pluton (Villaseca *et al.* 1995).

The La Cabrera pluton, covering 160 km², is another I-type massif that exhibits complex compositional variations. It shows an evolutionary trend from amphibole-bearing granodiorite at the margin toward biotite monzogranite as the dominant facies at the center (Bellido 1979). Some leucogranitic facies occur in the core. A Rb–Sr isochron age of 310 ± 14 Ma was obtained for the main monzogranite.

The La Pedriza pluton is one of the most felsic I-type plutons in the SCS. It is composed of coarse-grained biotite leucogranite outcropping in a 75 km² massif. It shows a cryptic geochemical zoning, with a strong increase in rare elements toward the northeastern margin, where it reaches the highest bulk-rock contents of Na–F–Rb–Hf–Th–U–Nb–Ta–Y–HREE. In some

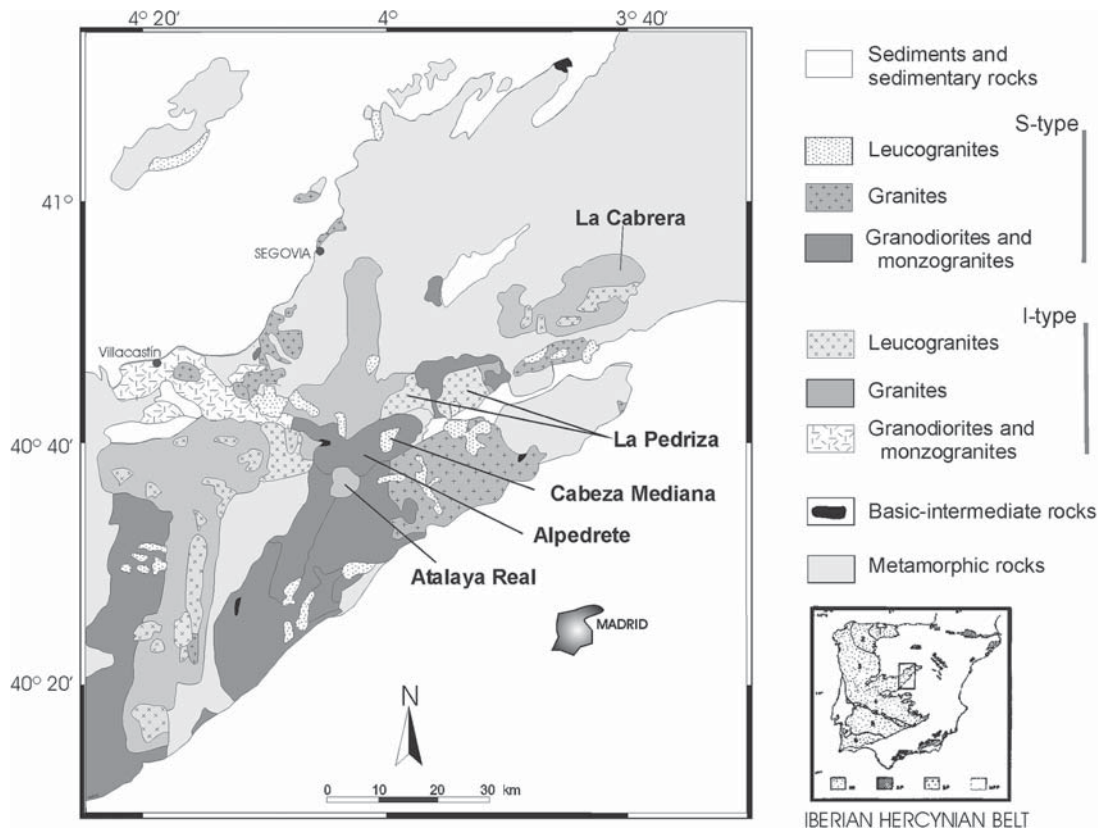


FIG. 1. Geological map of the Sierra de Guadarrama, in the Spanish Central System, showing the distribution and type of granite plutons considered in this study (modified after Villaseca *et al.* 1998).

marginal areas, aplitic to pegmatitic bodies appear. A Rb–Sr isochron age of 307 ± 3 Ma was reported for the pluton (Pérez-Soba 1992).

Two S-type plutons have been selected for this study. The cordierite-bearing Alpedrete pluton, a typical S-type granite, is an irregular massif covering an area of around 350 km^2 (Fig. 1). It is composed of equigranular cordierite-bearing granodiorite to monzogranite. Some attempts at Rb–Sr dating have failed, suggesting a heterogeneous isotopic character (Villaseca *et al.* 1995). It is intruded by younger circular plutons, such as the Atalaya Real I-type pluton. The Cabeza Mediana pluton is a two-mica leucogranite also intrusive in the Alpedrete pluton (Fig. 1); it forms a small circular pluton of 7 km^2 and is dated at 291 ± 6 Ma by Rb–Sr isochron.

ANALYTICAL METHODS

Wavelength-dispersion electron-microprobe (EPMA) analyses of zircon were carried out using a JEOL Superprobe JXA 8900–M equipped with four spectrometers

at the Microscopía Electrónica CAI, of the Universidad Complutense de Madrid. The EPMA was operated with an acceleration voltage of 20 kV and a probe current of 50 nA. Counting times were varied from element to element, in the range 10–30 s (peak) and 5–15 s (background). Zircon grains with too low an analytical total (discussed in detail below) were analyzed again, with a beam current of 150 nA and counting times for Zr, Hf, REE, U and Th extended to 100 s (peak) and 50 s (background). Under the latter conditions, detection limits (calculated from the three-fold background noise) were on the order of 100 ppm for most of these elements. The beam diameter was between 2 and $5 \mu\text{m}$ to minimize damage to the grains. Natural standards, including albite, kaersutite, almandine, zircon, vanadinite and REE phosphates, were used for most elements (Jarosewich *et al.* 1980, Jarosewich & Boatner 1991) except U and Th, for which commercial glasses were used. An on-line ZAF correction program was used. To examine the compositional heterogeneity of zircon, back-scattered-electron (BSE) imaging was used.

Cathodoluminescence (CL) imaging also is a powerful technique to reveal internal textures of zircon (*e.g.*, Hanchar & Miller 1993, Corfu *et al.* 2003). We found, however, that the majority of our zircon samples are virtually non-luminescent, which is why CL imaging was not applied in this study.

The degree of radiation damage of zircon was estimated from the FWHM (full width at half band-maximum) of the $\nu_3(\text{SiO}_4)$ Raman band (B_{1g} -type vibration) of this mineral, which is observed at about 1000 cm^{-1} (Nasdala *et al.* 1995, 2001a). Raman spectra were obtained by means of a Renishaw RM 1000 research-

grade Raman spectrometer. This notch-filter-based system is equipped with a Leica DMLM series optical microscope, a grating with 1200 grooves per millimeter, and a Si-based charge-coupled device detector. Because laser-induced photoluminescence may, as an analytical artefact, affect Raman spectra, especially in the green-yellow range of the electromagnetic spectrum (*e.g.*, Nasdala & Hanchar 2005), spectra were excited with the 6328 \AA emission of a He-Ne laser. The Leica $100\times$ objective (numerical aperture 0.95) was used. Confocal measurements were done with a lateral resolution of

TABLE 1. SUMMARY OF MAGMATIC MINERALOGY OF THE SCS HERCYNIAN PLUTONS STUDIED

Pluton		Texture	Major minerals	Accessory minerals
I-type granite				
Atalaya Real	granodiorite – monzogranite	equigranular, coarse grained	Qtz, Pl, Kfs, Bt	Hbl, Fap, Zrn, Ilm, Aln, Mnz, Xnt, Thr
	leucogranite	porphyritic, fine to medium grained	Qtz, Pl, Kfs	Bt, Hbl, Fap, Zrn, Ilm, Aln, Mnz, Xnt, Thr
	aplite	equigranular, fine grained	Qtz, Pl, Kfs	Bt, Hbl, Fap, Zrn, Ilm, Aln, Mnz, Xnt, U-Thr
La Cabrera	granodiorite – monzogranite	equigranular, coarse to medium grained	Qtz, Pl, Kfs, Bt	Hbl, Cpx, Fap, Zrn, Ilm, Mnz, Xnt, Aln
	leucogranite	equigranular, fine to medium grained	Qtz, Pl, Kfs	Bt, Fap, Zrn, Ilm, Mnz, Xnt, Aln, Fl, Ms
	aplite	inequigranular, fine grained	Qtz, Pl, Kfs	Bt, Fap, Zrn, Ilm, Mnz, Xnt, Grt
La Pedriza	leucogranite (western sector)	equigranular, coarse grained	Qtz, Kfs, Pl	Bt, Fap, Zrn, Ilm, Aln, Mnz, Xnt, Fl, Grt, Urn
	leucogranite (central sector)	equigranular, coarse grained	Qtz, Kfs, Pl	Bt, Ms, Fap, Zrn, Mnz, Xnt, Fl, Ilm, Thr, Mcl, Upc, Nb-Rt
	leucogranite (eastern sector)	equigranular, coarse grained	Qtz, Kfs, Pl	Bt, Fap, Zrn, Mnz, Xnt, Mgt, Fl, Thr
S-type granite				
Alpedrete	granodiorite – monzogranite	equigranular, fine to medium grained	Qtz, Pl, Kfs, Bt	Crd, Fap, Zrn, Ilm, Mnz, Xnt
Cabeza Mediana	leucogranite	equigranular, fine to medium grained	Qtz, Pl, Kfs	Bt, Crd, Ms, And, Sil, Fap, Zrn, Ilm, Mnz, Xnt, Urn, Tur

Mineral abbreviations according to Kretz (1983). Symbols of other minerals: Fap: fluorapatite, Mcl: manganocolumbite, Nb-Rt: Nb-rich rutile, Thr: thorite, Urn: uraninite, Upc: uranpyrochlore, U-Thr: uranoan thorite, Xnt: xenotime.

$\sim 2\text{--}3\ \mu\text{m}$. The wavenumber accuracy was $0.5\ \text{cm}^{-1}$, and the spectral resolution was $\sim 2\ \text{cm}^{-1}$.

PETROGRAPHIC FEATURES AND PATTERN OF ZONING IN THE ZIRCON

We recognize two main types of zircon in the SCS plutons studied, comparing both I- and S-type granites, according to zoning and textural characteristics. *Type 1*: Euhedral to subhedral crystals exhibit finely concentric oscillatory zoning in BSE imaging. These crystals commonly show an unzoned inner part and outer oscillatory bands (Figs. 2A to D). We have not found a clear inherited core (residual zircon?), and only rarely does this type contain inclusions of other minerals (Fig. 2C). About 75% of the zircon crystals are isolated, whereas the others form clusters with xenotime, thorite, monazite or apatite. Type-1 crystals are mainly included in biotite, occasionally in quartz or K-feldspar, and exceptionally they are hosted in plagioclase (4%). This type of zircon appears mainly in granodiorite and monzogranite plutons, but also can be found in minor amounts in leucogranites (Table 2).

Type-2 zircon forms subhedral to anhedral unzoned or irregularly zoned crystals (Figs. 2E to I). About 60% of these crystals form clusters with other accessory minerals, such as xenotime, thorite, apatite or monazite. These crystals occur mostly as inclusions at the rim of the biotite (less frequently than in type 1) and sodic plagioclase (20%), or as intergranular crystals among quartz, the feldspars or biotite. Type-2 zircon is typically found in leucogranites, aplites and pegmatites, and is less abundant in granodiorites and monzogranites (Table 2). Three subtypes are distinguished according to their pattern of zoning. Type 2a, the alveolar subtype, is

the main one, characterized by the presence of domains rich in micro-inclusions with homogeneous or irregular zoning. These micro-inclusions may extend all over the grain (in about 80% of the crystals) (Figs. 2H, E), and more rarely are restricted to an inner domain (Fig. 2G) or to an outer rim. Type 2a is texturally similar to zircon described by Romans *et al.* (1975), Rubin *et al.* (1989) and Uher & Černý (1998). The micro-inclusions are irregular crystals (usually $< 2\ \mu\text{m}$ in length) of thorite or xenotime, or larger crystals of rock-forming minerals (biotite and plagioclase), ranging up to $20\ \mu\text{m}$ in length. Type-2a zircon is included mainly in biotite and, less commonly, in plagioclase. In plagioclase, the zircon crystals are isolated, whereas in biotite they usually appear to be associated with xenotime, thorite and monazite. This type of zircon mainly appears in leucogranite and aplitic granite, being especially widespread in the La Pedriza leucogranite (Table 2).

Type 2b crystals are homogeneous, unzoned or with very weak (diffuse) sector-zoning. The sections are subhedral to euhedral. Crystals usually occur inside biotite and plagioclase, and can be found both isolated crystals or grouped with xenotime and thorite, or less commonly with apatite and monazite. This subtype is most common in monzogranites and granodiorites.

Type 2c crystals constitute the complex subtype; the crystals exhibit areas with oscillatory, simple or patchy zoning. Moreover, some of the interior regions may be alveolar, suggesting transitions between all these subtypes of zircon (Fig. 2I). In the Atalaya Real aplites, some of these crystals show eccentric and strikingly corroded cores (Fig. 2F), although commonly the distinct sector-zoning has a concentric distribution. Most of these type-2c crystals are hosted in biotite.

Zircon of types 1 and 2 has not been found in the same host mineral, but could appear in the same thin section. These types of zircon also contrast in terms of two morphological parameters, the longest dimension of the grain and the elongation (width / length). Geometrical features based on thin-section studies underestimate the real greatest dimension of the zircon crystals and also their elongation ratio, but for comparative purposes, these may be considered a good estimate. Figure 3 shows geometrical parameters for the two types of zircon and for the three main subgroups of lithologies. Although in some cases the number of data points is low owing to the scarcity of zircon in the samples, some tendencies can be deduced using such a graphical analysis, as discussed in Higgins (1994). The frequency distribution of both parameters in type-1 zircon from monzogranite and granodiorite plutons (Fig. 3) is indicative of elongate and large crystals. The type-2 zircon from leucogranites shows more equant and shorter sections than those of type-1 zircon, although a value of $250\ \mu\text{m}$ for a single-crystal length was established. Moreover, the shortest crystals of the zircon population ($\leq 20\ \mu\text{m}$) are present in the La Pedriza leucogranite. Type-2 zircon in aplites is

TABLE 2. FREQUENCY OF OCCURRENCE OF ZIRCON TYPES IN THE SCS HERCYNIAN PLUTONS STUDIED

Pluton		<i>n</i>	1	2a	2b	2c
I-type plutons						
Atalaya Real	granodiorite–monzogranite	47	79	21	-	-
	leucogranite	22	23	36	23	18
	aplite	21	-	43	38	19
La Cabrera	granodiorite–monzogranite	38	97	-	3	-
	aplite	8	38	25	25	12
	pegmatite	6	-	67	33	-
La Pedriza	leucogranite	112	30	15	36	19
S-type plutons						
Alpedrete	granodiorite–monzogranite	21	71	19	-	10
Cabeza Mediana	leucogranite	12	42	33	-	25

Zircon types: 1: euhedral, elongate crystals, with oscillatory zoning; 2a: alveolar, 2b: homogeneous, 2c: complex subtype. The frequency of zircon types is reported in %; *n*: number of crystals sampled.

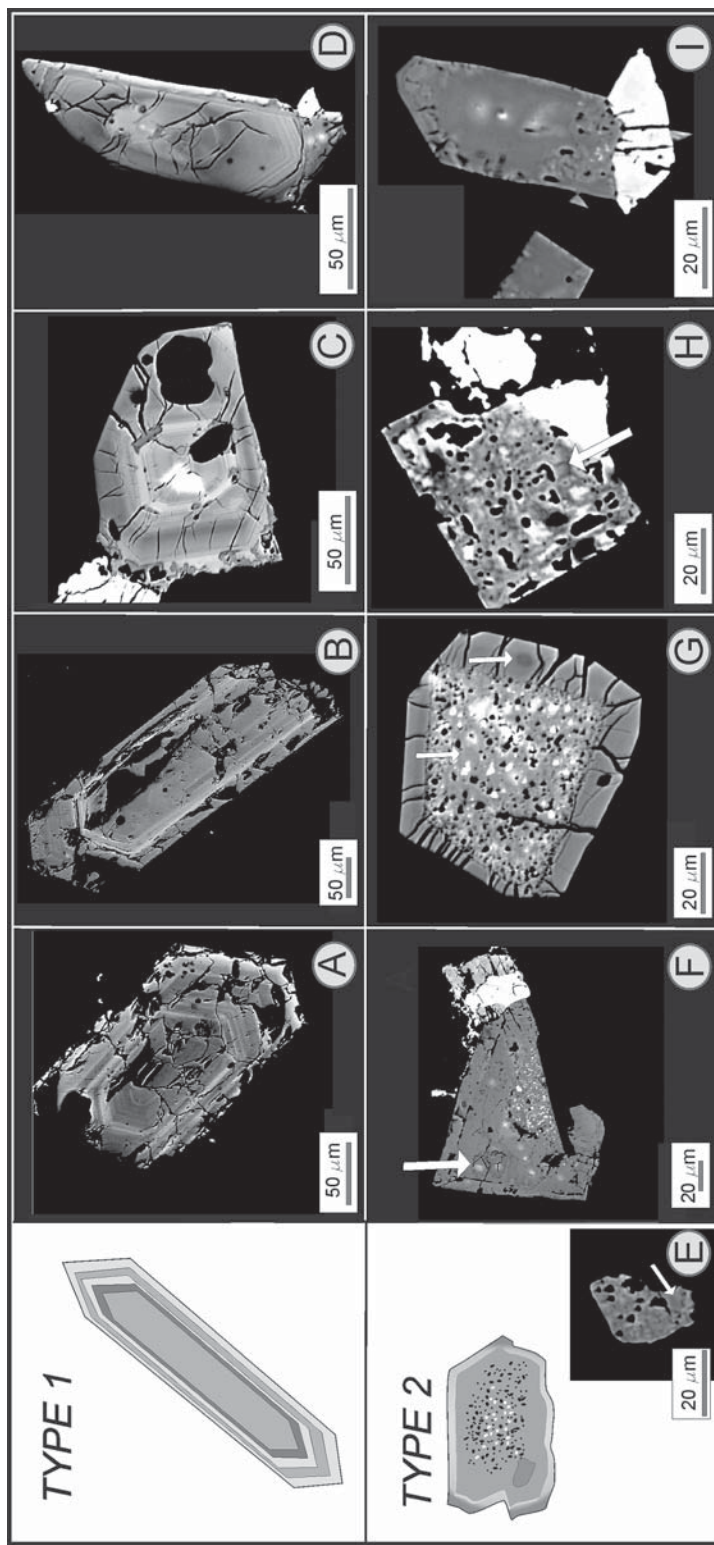


Fig. 2. Back-scattered electron images of different types and subtypes of zircon distinguished in this work. Type-1 zircon: A) Elongate crystal showing oscillatory zoning (Atalaya Real granodiorite, s. 95922). B) Common crystal of type 1 (La Pedriza leucogranite, s. 67065). C) Euhedral transversal section of type-1 zircon, with characteristic oscillatory zoning. D) Subhedral section of type-1 zircon, showing oscillatory zoning, weakly contrasted. Type-2 zircon: E) Subtype 2b (alveolar): common crystal of alveolar subtype, in this case with irregular inclusions of plagioclase. The arrow points to the spot of the composition with $\text{SiO}_2 = 31.65$ wt.% (Table 3); (La Pedriza leucogranite, s. 87059) F) Subtype 2c (complex): crystal with alveolar center showing an eccentric nucleus (arrow) with a composition $\text{SiO}_2 = 24.83$ wt.% in Table 3, in a wide unzoned central sector (Atalaya Real aplite, s. 96922). G) Subtype 2b (alveolar): zoned crystal with an alveolar center (rich in bright and opaque inclusions, composition with $\text{SiO}_2 = 28.84$ wt.% in Table 3) and a homogeneous rim ($\text{SiO}_2 = 31.35$ wt.% in Table 3) (La Pedriza leucogranite, s. 87225). H) Subtype 2b (alveolar): euhedral transversal section of zircon rich in irregular inclusions; area (marked by the arrow) with a deficient analytical total (composition with $\text{SiO}_2 = 28.76$ wt.% in Table 3) (La Pedriza leucogranite, s. 87166). I) Subtype 2c (complex): zoned crystal with a small alveolar sector in a mainly homogeneous inner zone and a rim with subtle oscillatory growth-zoning; the bright crystal is xenotime (La Pedriza leucogranite).

mostly equidimensional, but is not shorter than those belonging to leucogranites. This tendency clearly changes for type-2 zircon from La Cabrera pegmatites (not included in these diagrams), which reach lengths up to 800 μm , with elongation ratio between 0.1 and 0.2 (acicular varieties).

COMPOSITION AND STRUCTURAL STATE OF ZIRCON IN THE GRANITIC ROCKS

Nearly 125 EPMA analyses of type-1 zircon and about 240 analyses of type-2 zircon were made. Representative EPMA results are shown in Table 3. Internal zoning is mainly related to variations of Hf, Y, HREE, U and Th concentrations; these elements are therefore considered to be the main indicators of degree of evolution and differences among types of zircon. The contrast in the compositional range of type of zircon is expressed in Figure 4 according to plutons and degree of differentiation.

In granodiorite and monzogranite, both types of zircon define low values in the oxides considered, whereas the most felsic varieties (leucogranites, aplites and pegmatites) have higher medians and reach the highest contents of Hf, Y, HREE, Th and U. This is displayed by I-type granites and, to a lesser degree, by S-type granites, perhaps related to the lack of aplite-pegmatite dykes in these plutons.

Type-1 zircon usually has the lowest contents in U, Th, Y, HREE and Hf, and displays a narrower compositional range than type-2 zircon. The compositional range of type-1 zircon is independent of their host (leucogranite to granodiorites, Fig. 4), as found in other studies (Wang *et al.* 2000). Compositional ranges in type-1 zircon are (in wt.%): 0.51–5.75% HfO_2 , 0–4.03% UO_2 , 0–1.65% ThO_2 , 0–4.12% Y_2O_3 and 0.21–2.35% HREE_2O_3 . The zoning defined in type-1 single crystals

is different in the less and the more evolved granites. In zircon from granodiorite and monzogranite samples, a positive correlation of Hf, U, Th, Y and HREE concentration is usually observed, which generally increases from core to rim, whereas in the evolved granites, levels of U, Th, Y and HREE decrease and Hf increase toward the rim.

The type-2 zircon from leucogranite and aplite has a more variable composition (Fig. 4), with higher contents of HfO_2 (13.60 wt.%), UO_2 (4.83%), ThO_2 (4.87%), Y_2O_3 (8.51%) and HREE_2O_3 (3.78%) and the lowest analytical totals (91.17 wt.%) (Table 3). Zircon from the La Cabrera pegmatites shows the highest HfO_2 contents (16.58 wt.%). In type-2 zircon, the compositional ranges among the three subtypes in general show a great overlap (Table 3), although type-2b zircon from the La Cabrera pegmatites shows the highest Hf content, and type-2c zircon from the Atalaya Real aplites (Fig. 4) shows the highest Th, Y and HREE contents. Alveolar subtype-2a is richer in Th and poorer in Hf in those areas with thorite micro-inclusions. About half of the population of zoned type-2 zircon displays significant covariation in U, Th, Y and HREE contents (similar to that described by Pointer *et al.* 1988, Wang *et al.* 2000, Mathieu *et al.* 2001, Fowler *et al.* 2002), whereas in most cases, Hf displays an opposite behavior, which contrasts with findings in other studies (*e.g.*, Uher & Černý 1998, Wang *et al.* 2000, Belousova *et al.* 2002).

The compositional zoning in subtype-2 zircon usually shows the same trend, defined by a decrease in levels of U, Th, Y, HREE toward rim, whereas Hf increases. Nevertheless, alveolar crystals are irregularly zoned; only where the alveolar domain is rimmed by a homogeneous growth, the inner zone is richer or similar in content to the rim (Fig. 2G). Subtype 2b usually shows the general compositional path defined for type 2, showing the largest range of U contents. In subtype-2c

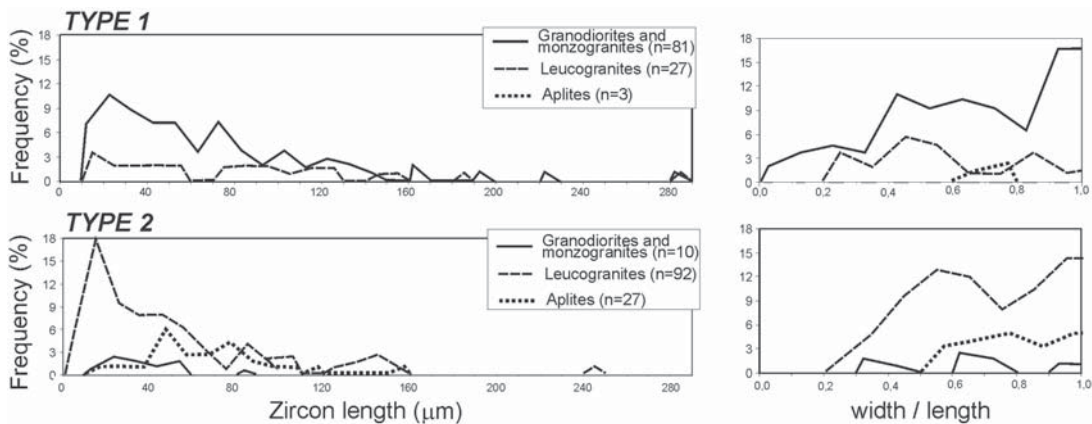


FIG. 3. Histograms of length (L_{max}) and elongation (width/length) in zircon of type 1 and 2. For each category, the percentage of the main rocks to the total of the population is compared.

TABLE 3. REPRESENTATIVE RESULTS OF EPMA ANALYSES OF ZIRCON CRYSTALS IN THE PLUTONS STUDIED

Type	Pluton	Granite	Sample	SiO ₂	ZrO ₂	P ₂ O ₅	HfO ₂	Y ₂ O ₃	HREE	ThO ₂	UO ₂	Al ₂ O ₃	FeO	CaO	MnO	MgO	Total
1	La Cabr.	Monzog.	52530 c	33.02	64.19	0.04	1.34	0.05	0.28	<0.02	0.07	<0.01	0.09	<0.01	n.d.	n.d.	99.24
1	La Cabr.	Monzog.	52530 r	33.24	63.40	0.09	1.65	0.16	0.29	0.05	0.26	<0.01	0.10	<0.01	n.d.	n.d.	99.45
1	La Cabr.	Aplite	55840 c	29.26	54.15	0.88	1.21	2.55	1.43	1.65	3.68	<0.01	0.09	0.71	n.d.	n.d.	94.81
1	La Cabr.	Aplite	55840 r	30.02	57.24	1.03	2.09	2.19	1.52	0.77	3.03	<0.01	0.09	0.45	n.d.	n.d.	98.63
1	La Pedr.	Leucogr.	87225 c	31.39	60.68	0.34	0.89	1.41	0.78	1.12	0.87	<0.01	0.06	<0.01	<0.02	<0.01	97.79
1	La Pedr.	Leucogr.	87225 m	32.18	64.81	0.17	1.71	0.28	0.19	0.07	0.38	<0.01	0.09	<0.01	<0.02	<0.01	100.05
1	La Pedr.	Leucogr.	87225 r	30.19	56.67	0.81	2.23	1.27	0.75	0.19	2.05	0.16	1.02	2.57	0.13	<0.01	98.21
1	La Pedr.	Leucogr.	86822 c	28.33	55.07	1.01	1.88	1.57	0.91	0.39	2.33	0.18	0.23	2.69	0.17	<0.01	95.01
1	La Pedr.	Leucogr.	86822 r	30.61	65.31	0.11	2.30	0.09	0.27	0.05	0.22	<0.01	0.14	<0.01	<0.02	<0.01	99.29
1	La Pedr.	Leucogr.	86822	31.51	62.43	0.44	2.83	0.58	0.64	0.06	0.53	0.06	0.71	0.06	<0.02	0.02	100.09
1	A. Real	Granod.	96026 c	30.42	64.29	0.16	1.57	<0.02	0.31	<0.02	<0.01	<0.01	0.08	0.02	<0.02	<0.01	97.08
1	A. Real	Granod.	96026 m	30.15	63.75	0.33	1.75	0.61	0.53	0.18	0.86	<0.01	n.d.	<0.01	<0.02	<0.01	98.37
1	A. Real	Granod.	96026 r	28.03	54.13	1.08	1.81	1.82	1.20	0.47	2.80	0.13	0.85	3.00	0.06	<0.01	95.59
1	A. Real	Granod.	95922	31.48	67.14	0.11	1.26	0.10	0.20	0.03	0.02	<0.01	<0.02	<0.01	<0.02	<0.01	100.53
1	Alpedr.	Monzog.	95918 c	31.18	64.32	0.32	0.94	0.35	0.56	0.05	0.02	<0.01	0.14	0.03	n.d.	n.d.	98.25
1	Alpedr.	Monzog.	95918 r	29.77	65.11	0.59	1.59	0.56	0.44	0.04	0.34	<0.01	0.21	0.15	n.d.	n.d.	99.22
1	C. Med.	Leucogr.	76873	33.60	64.15	0.17	1.78	0.20	0.25	0.03	0.04	<0.01	0.07	<0.01	n.d.	n.d.	100.63
1	C. Med.	Leucogr.	76873	28.78	57.82	3.02	0.91	4.12	1.84	0.52	0.93	<0.01	0.06	<0.01	n.d.	n.d.	98.43
2a	La Cabr.	Aplite	55840	31.34	57.85	0.55	1.75	1.27	1.15	1.29	1.66	0.13	0.03	0.29	n.d.	n.d.	97.47
2b	La Cabr.	Aplite	55840	27.63	53.21	1.38	1.27	3.17	1.74	1.73	4.19	0.03	0.03	0.76	n.d.	n.d.	95.30
2c	La Cabr.	Pegm.	c	28.85	44.56	0.32	15.94	1.73	1.35	0.28	1.47	0.24	0.31	0.28	n.d.	n.d.	95.94
2c	La Cabr.	Pegm.	r	28.74	44.94	0.64	16.58	1.84	1.07	0.49	1.75	0.13	0.36	0.32	n.d.	n.d.	97.47
2a	La Pedr.	Leucogr.	87225 c	28.84	56.00	1.32	1.13	1.84	1.38	0.90	2.09	0.17	0.99	2.99	0.07	0.01	98.10
2a	La Pedr.	Leucogr.	87225 r	31.35	66.43	0.06	1.40	0.08	0.19	<0.02	<0.01	<0.01	0.30	<0.01	<0.01	<0.01	99.97
2b	La Pedr.	Leucogr.	87225	27.73	52.65	1.16	2.51	2.31	1.46	0.20	4.83	0.11	1.05	1.64	0.20	<0.01	96.10
2a	La Pedr.	Leucogr.	87225	28.84	56.00	1.32	1.13	1.84	1.52	0.90	2.09	0.17	0.99	2.99	0.07	<0.01	98.10
2a	La Pedr.	Leucogr.	67263 c	26.82	54.78	0.64	3.44	1.77	1.26	0.20	3.33	0.54	0.47	1.51	0.31	0.02	95.33
2a	La Pedr.	Leucogr.	67263 r	26.59	45.36	0.96	13.60	1.41	1.75	0.58	2.91	0.17	0.31	0.87	0.19	0.03	94.91
2a	La Pedr.	Leucogr.	87059	31.65	62.64	0.16	3.71	0.16	0.50	<0.02	0.14	0.06	0.05	0.03	<0.02	<0.01	99.23
2a	La Pedr.	Leucogr.	87166	28.76	57.37	0.41	2.43	0.68	2.24	0.05	1.13	<0.01	2.01	1.33	0.91	<0.01	96.38
2a	A. Real	Leucogr.	96022	29.57	59.49	0.25	1.60	0.76	0.60	0.93	1.75	0.10	1.24	0.87	0.25	<0.01	97.36
2a	A. Real	Leucogr.	96024	30.89	62.58	0.27	3.32	0.38	0.58	0.06	0.92	0.05	0.36	0.44	<0.02	0.02	100.05
2b	A. Real	Leucogr.	96024 c	32.23	66.86	0.07	1.20	0.07	0.22	<0.02	<0.01	<0.01	0.05	<0.01	<0.02	<0.01	100.96
2b	A. Real	Leucogr.	96024 r	32.00	65.18	0.14	1.27	0.66	0.61	0.14	0.37	0.02	0.06	0.02	<0.02	<0.01	100.71
2c	A. Real	Aplite	96027 c	24.83	42.13	0.80	0.60	8.51	3.74	4.72	2.53	1.53	0.72	2.24	0.05	0.06	93.37
2c	A. Real	Aplite	96027 r	27.65	54.65	0.89	0.79	2.58	1.24	1.20	3.10	0.31	0.03	2.43	<0.02	<0.01	95.19
2c	A. Real	Aplite	96027 c	23.36	43.56	0.97	0.54	7.60	3.78	4.87	1.71	1.24	0.80	1.84	0.03	0.06	91.17
2c	A. Real	Aplite	96027 r	30.09	56.78	1.07	1.27	3.05	1.80	1.62	1.50	0.17	0.09	0.13	<0.02	<0.01	97.87
2b	Alpedr.	Monzog.	95918	31.15	64.09	0.66	1.38	0.49	0.66	0.04	0.07	0.04	<0.02	0.05	n.d.	n.d.	98.93
2b	C. Med.	Leucogr.	76873 c	30.45	61.38	0.71	1.40	1.08	0.68	0.34	0.68	0.04	0.52	0.36	n.d.	n.d.	98.11
2b	C. Med.	Leucogr.	76873 r	32.01	63.28	0.43	1.37	0.56	0.58	0.05	0.25	<0.01	0.46	0.02	n.d.	n.d.	99.42

Oxides in wt.%. Zircon types: 1: euhedral, elongate crystals, with oscillatory zoning; 2a: alveolar, 2b: homogeneous, 2c: complex subtype; c: core, m: middle, r: rim, n.d.: not determined. HREE: oxides of Gd + Dy + Er + Yb + Lu.

zircon, the corroded cores from the Atalaya Real aplites show the highest Th (4.7 to 4.9 wt.% ThO₂), Y (7.6 to 8.5 wt.% Y₂O₃) and HREE (3.7 to 3.8 wt.% HREE₂O₃) contents, whereas Hf increases toward the rim. This Hf increase toward the rim of a single crystal of zircon is common in our collection of types and is also extensively recognized in other studies (*e.g.*, Hanchar & Miller 1993, Uher *et al.* 1998, Pupin 2000).

Transgressive rims in type-2 zircon do not modify the common zoning defined for this type of zircon; only Ca and Al are appreciably lost. This contrasts with the loss of trace elements in transgressive rims described by Pidgeon *et al.* (1998), and also by Geisler *et al.* (2003a) in experiments of zircon alteration at low temperatures.

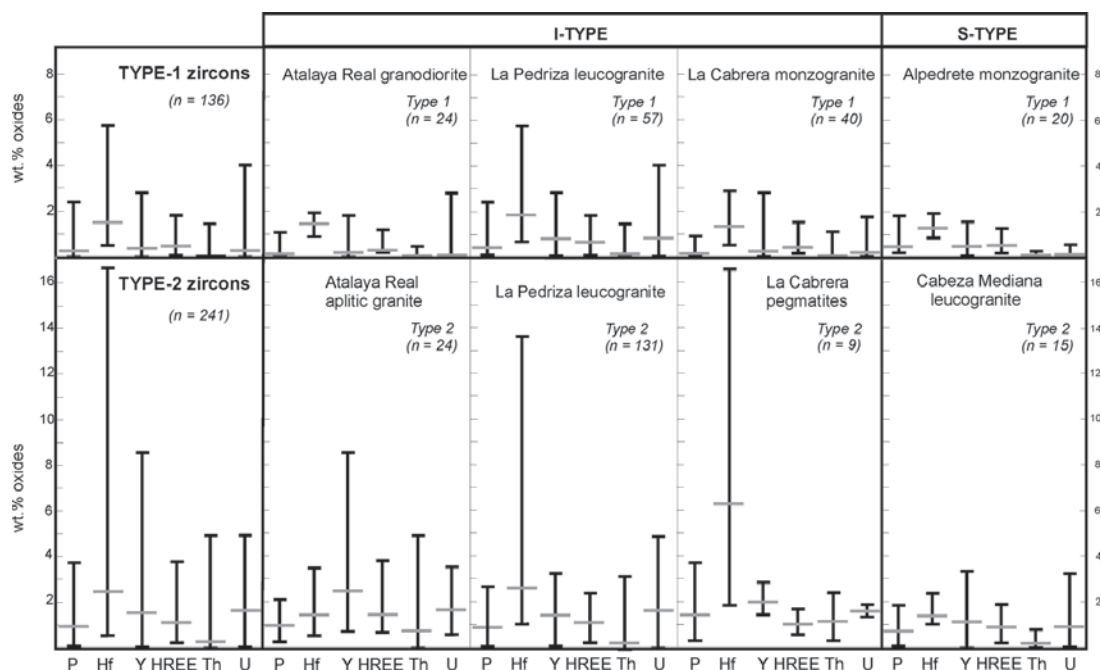


Fig. 4. Compositional comparison between zircon of types 1 and 2 from representative SCS granitic plutons. Bar shows the complete range of zircon composition (vertical line), including the median (short horizontal line). Oxides expressed in wt.%.

Figure 5 shows the different Th/U paths in our zircon. Most zircon grains from monzogranite or granodiorite (irrespectively of their zircon type) show a Th:U ratio of approximately 0.1. Type-1 zircon in granodiorite and monzogranite shows a more restricted range of values compared with the zircon (types 1 and 2) in more evolved granites. Zircon of these felsic granites usually show a higher Th:U ratio, which seems to be pluton-dependent. Thus, in the La Pedriza pluton, most of the zircon crystals (irrespectively of type) also show a Th:U ratio close to 0.1, whereas type-1 zircon from the La Cabrera aplite shows a Th:U ratio near 1, and type-2c zircon from the Atalaya Real aplite shows a Th:U ratio near 2 (Fig. 5).

Shortfalls in analytical totals (considered as less than 98 wt.%) are found in about 30% of type-1 zircon population and in 50% of the type-2 population; the latter population shows the lowest analytical totals found. The mean of the analytical totals of corroded cores of subtype 2c shows lower values (96.11 wt.%) than types 2a (~97.7 wt.%). In these crystals, the structural state of zircon, *i.e.*, the degree of metamictization, was studied by means of Raman spectroscopy (Nasdala *et al.* 1995). Figure 6 shows a typical Raman spectrum as obtained in this study, in comparison with two reference spectra of the poorly radiation-damaged Curtin University (Perth) ion-probe standard CZ3 and

a well-crystallized synthetic crystal of zircon. We found that our zircon samples do generally show high levels of radiation damage, which is indicated by FWHM values [$\nu_3(\text{SiO}_4)$ Raman band] exceeding 30 cm^{-1} , and low band-intensities (Fig. 6). Such extensive band-broadening is considered to correspond to an amorphous volume-fraction exceeding 60–70% (Zhang *et al.* 2000, Zhang & Salje 2001), which characterizes our areas of low analytical total as strongly metamict.

DISCUSSION

Cation substitutions

Zircon conforms to the general formula ABO_4 , where the position *A* represents the relatively large zirconium ion in eight-fold coordination with O, and position *B* represents the silicon ion in tetrahedral coordination with O. In position *A*, Zr can be replaced by tetravalent ($M^{4+} = \text{Hf, Th, U}$), trivalent ($M^{3+} = \text{REE, Y, Fe}$), and divalent cations ($M^{2+} = \text{Ca, Fe, Mg, Mn}$). As summarized by Hoskin & Schaltegger (2003), there are multiple mechanisms of substitution, including simple isovalent replacement of Zr by other tetravalent cations, and coupled substitutions where divalent and trivalent cations may be incorporated.

Solid solution toward xenotime plays an important role in zircon composition. The proportion of M^{3+} cations at the A site must be similar to the proportion of P^{5+} at the B site, according to the coupled-substitution mechanism (Y + HREE)P Zr₋₁ Si₋₁ (e.g., Speer 1980, Hanchar *et al.* 2001). The close correlation between Zr + Hf and Th + U allows us to consider total M^{4+} cations (Zr + Hf + U + Th) instead of Zr (as has been proposed by Fowler *et al.* 2002). In that way, most of the zircon samples plot along the vector 1:1 representative of A-site substitution for M^{3+} cations (Fig. 7A). On the other hand, the coupled (P + Al) for Si substitution plots closer to the 1:1 line than P alone, which is suggestive of preferential Al incorporation at this site (Fig. 7B), as stated by Uher & Černý (1998) and Akhtar & Wassem (2001). This substitution is shown by all the groups of zircon, although some type-2 zircon samples are situated below this line, indicating in these cases some deficiency in P.

Divalent cations like Ca, Fe and Mn also may be present in zircon, occupying interstitial sites. These M^{2+} cations have been considered as involved in the xenotime–zircon series, providing a mechanism of charge balance for the HREE and Y in excess of P: $(Mg, Fe)^{2+}_{(int)} + 3(Y, HREE)^{3+} + P^{5+} = 3Zr^{4+} + Si^{4+}$ (Romans *et al.* 1975, Hoskin *et al.* 2000). This fact

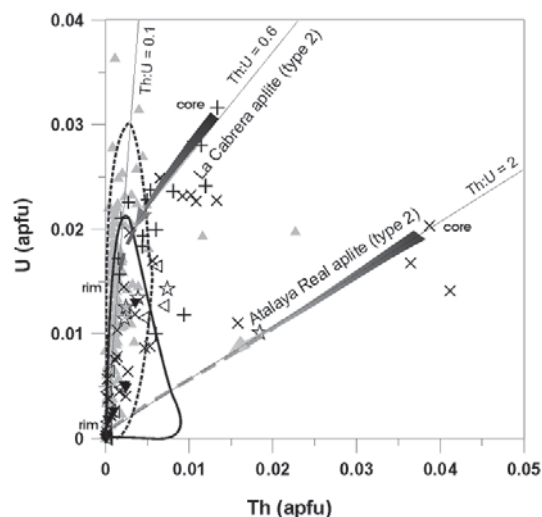


FIG. 5. Variation in amount of U versus Th in zircon crystals. Diagonal lines representing Th:U ratios of 0.1, 0.6 and 2 are shown. The compositional range of zircon of type 1 and type 2 from monzogranites and granodiorites (MzGr), and zircon of type-1 from leucogranites and aplites (LAP) are enclosed in areas. Arrows define the compositional zoning in a single crystal. Symbols for type-2 zircon are as follows: ☆ La Cabrera pegmatite, + La Cabrera aplite, × Atalaya Real aplite, ◁ Atalaya Real leucogranite, △ La Pedriza leucogranite, ▼ Cabeza Mediana leucogranite.

reflects the inability of the Si site to incorporate enough P to charge-balance the REE³⁺ ions (Finch *et al.* 2001). On the other hand, studies of alteration in zircon show that these elements (specially Ca and Fe, but also Al and Ti) may be secondarily enriched in the altered zones of zircon crystals (Geisler & Schleicher 2000, Mathieu *et al.* 2001, Zhang *et al.* 2003, Geisler *et al.* 2003a, b, Johan & Johan 2004, Kempe *et al.* 2004). For example, Geisler *et al.* (2003a) studied experimentally the interaction of metamict zircon with hydrothermal fluids, and they observed a gain of solvent cations (e.g., Ca, Ba) from the hydrothermal solution, and the loss of variable amounts of M^{4+} cations (Zr, Si, Hf, Th, U) as well as M^{3+} cations (REE). On the other hand, the REE incorporated in zircon have been considered essentially immobile by Cherniak *et al.* (1997). In this sense, significant correlations of REE versus (Ca + Fe) contents may indicate a primary (*i.e.*, magmatic) origin of the divalent cations Ca²⁺ and Fe²⁺. Figure 8A shows such correlation for most of the plutons studied, except for some analyses of monzogranites or aplites

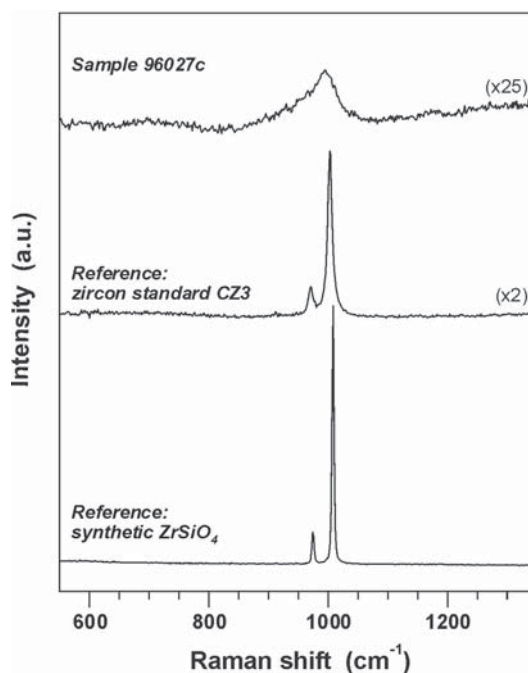


FIG. 6. Raman spectrum of a micro-area in zircon in aplite from the Atalaya Real pluton, whose electron-microprobe analysis gave a deficient total (96027c in Table 3). It is shown in comparison with spectra of the moderately radiation-damaged CZ3 zircon (Nasdala *et al.* 2001b) and well-crystallized, synthetic zircon (Nasdala *et al.* 2002). Spectra are stacked for clarity. Broadening and extremely low intensities of Raman bands characterize sample 96027c as strongly radiation-damaged.

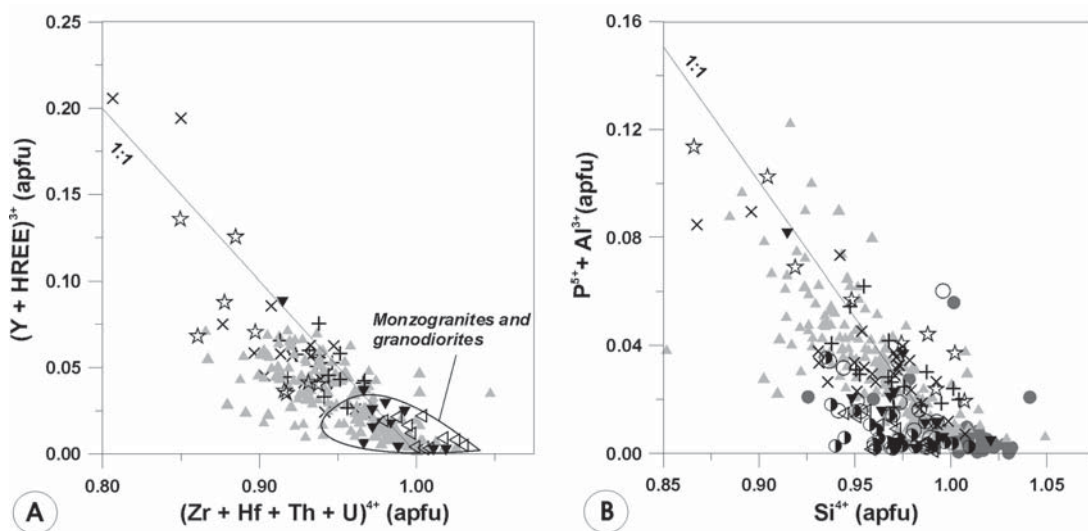


FIG. 7. Diagrams showing the extent of solid solution toward xenotime in zircon crystals in SCS granites (in atoms per formula unit: *apfu*). A) A-site substitution: $(\text{Zr,Hf,Th,U})^{4+}$ versus $(\text{Y,REE})^{3+}$ diagram. B) B-site substitution: Si^{4+} versus $(\text{P}^{5+} + \text{Al})$ plot. Area encloses zircon crystals of types-1 and 2 from monzogranites and granodiorites, and the diagonal line indicates the 1:1 substitution line. Same symbols as in Figure 5.

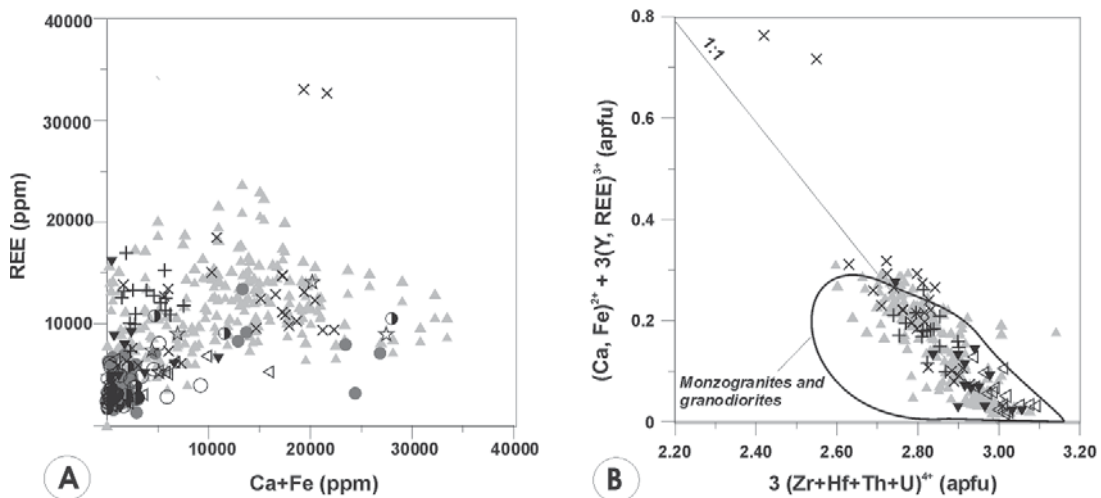


FIG. 8. Zircon plots. A) $(\text{Ca}^{2+} + \text{Fe}^{2+})$ versus REE plot. B) $3(\text{Zr,Hf,Th,U})^{4+}$ versus $(\text{Ca,Fe})^{2+} + 3(\text{Y,REE})^{3+}$ substitution diagram in zircon of types 1 and 2. The diagonal line indicates 1:1 substitution line. The compositions are expressed in atoms per formula unit (*apfu*). Same symbols as in Figure 5.

and a group of analyses of type-1 and -2 zircon from La Pedriza. In these cases, part of the Ca + Fe contents could be gained in the alteration processes. Except for these groups of compositions (around 40), we consider that Ca and Fe are mainly magmatic in origin. This argument is supported where the xenotime substitution

is represented, including all M^{4+} and M^{2+} cations at the A site (Fig. 8B). In this plot, most of the zircon data fall along the 1:1 line, suggesting that the incorporation of M^{2+} cations is related mainly to a magmatic mechanism of substitution.

Some differences in the degree of replacement of Zr by M^{2+} , M^{3+} and M^{4+} cations seem to depend upon their host-granite type. Thus, zircon from S-type granites does not show appreciable substitution of (Th + U) for Zr, and the degree of any cation substitution is less important. A decrease in Th content is a typical trend in S-type granites, contrary to that in I-type varieties, which combined with their higher P content, favors xenotime crystallization instead of Th incorporation in zircon (Villaseca *et al.* 1998).

Zircon growth: implications from their textural and chemical characteristics

Textural and chemical contrasts between the two types of zircon and their different modal proportions with granite evolution suggest differences in growth conditions. Oscillatory zoning in zircon has been intensively studied (*e.g.*, Vavra 1994, Hoskin 2000), and a magmatic origin is suggested. Type-1 zircon seems to have crystallized during changing magmatic conditions, and is probably not an early liquidus phase (it rarely appears included in the core of plagioclase).

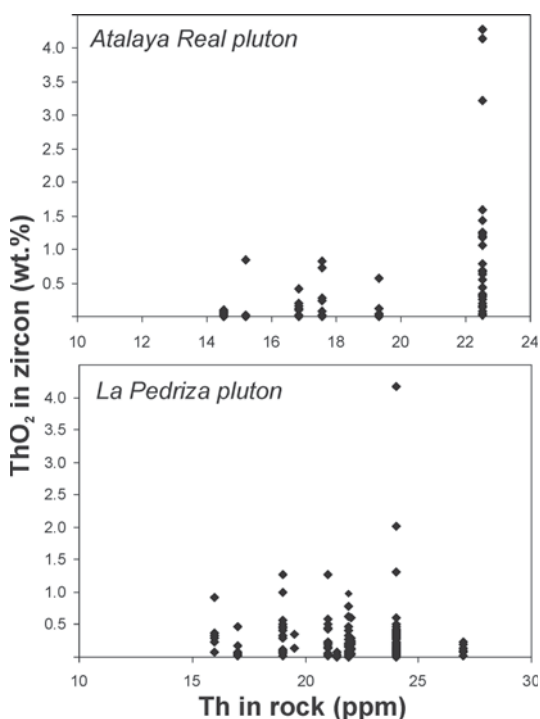


FIG. 9. Plot of Th in whole rock *versus* amount of ThO_2 in zircon from granites of the Atalaya Real and La Pedriza plutons. Data points represent the compositional range of ThO_2 contents in zircon crystals from a single thin-section.

On the other hand, most crystals of type-2 zircon likely grew at a late-magmatic stage because they show some faces (*i.e.*, are subhedral) and they grew simultaneously with the major phases (*e.g.*, biotite, the feldspars and quartz).

The Th-, U-, Y- and HREE-rich zircon is confined mainly to type-2 crystals from leucogranites, aplites and pegmatites. Its crystallization in the most evolved granitic magmas, which show enrichment in these elements, explains why its composition departs progressively from the ideal one. At the same time, the Th, U, Y, HREE and Hf contents are broadly correlated with the whole-rock composition (Fig. 9). Thus, the most-enriched zircon appears in the most fractionated granites.

As the level of incompatible trace-elements increases in felsic granitic melts, zircon incorporates other elements in addition to Hf. The decrease of Th–U–Y–HREE contents usually shown by type-2 zircon would suggest cocrystallization with accessory phases rich in Y and HREE (garnet, xenotime), or rich in U and Th (uraninite, thorite, monazite, allanite). Indeed, the presence of micro-inclusions of thorium-bearing minerals in the core area of these zircon crystals (Fig. 2G) suggests an environment saturated in Th-bearing phases (Černý & Siivola 1980). The cocrystallization of thorite contributes to a marked decrease of the total Th content in the outer part of the zircon crystals, although to a lower degree than stated in other studies (Lumpkin & Chakoumakos 1988, Wang *et al.* 1996), as spot analyses in “alveolar” sectors give still higher Th contents (up to 1.82 wt.%). The various patterns of trace-element zoning in zircon may also reflect the delicate balance in the more immediate environment of crystallization (*e.g.*, Rubin *et al.* 1989, Heaman *et al.* 1990, Wang *et al.* 1996), in view of competition with other accessory phases.

Finally, postmagmatic events (hydrothermal alteration of metamict zircon) may introduce Ca, Fe (Geisler & Schleicher 2000), together with U (Kempe *et al.* 2004) and with Hf and Y (Pointer *et al.* 1988, Uher *et al.* 1998). As we have seen above, the positive correlation between some of these cations (in our study, Ca, Fe and Mg) and those considered as being magmatic for most of plutons (Fig. 8A) suggests that these cations may be mainly incorporated at the magmatic stage.

The question of low analytical totals

In the plutons studied, zircon crystals or micro-areas within crystals with low analytical totals, in the range of 91–98 wt.%, have been found. This was observed in both type-1 and type-2 zircon samples, with type-2 zircon showing the phenomenon more commonly. Such domains (especially in the core and inner regions of zoned type-2 crystals) reveal the highest contents of Y, HREE, U and Th (Table 3).

Zircon samples yielding such unusually low analytical totals seem to occur quite rarely. Examples have been described from several localities worldwide (Peterman *et al.* 1986, Pointer *et al.* 1988, Smith *et al.* 1991, Irber *et al.* 1997, Kempe *et al.* 2000, Geisler *et al.* 2003b, Breiter *et al.* 2006). Low totals have mostly been reported from altered and significantly metamict zircon. As has already been discussed, the “low-total” zircon is commonly characterized by a particularly low BSE intensity (Kempe *et al.* 2000), which was confirmed in our material (Fig. 2).

Causes of the analytical shortfall and the related low BSE intensities are still hotly debated. In most of the above papers, authors have attempted to explain the low totals by the incorporation of hydrous species (which are not analyzed in the electron microprobe and may in addition cause phase degradation under the electron beam). Alternatively, enhanced quantities of vacancies (Kempe *et al.* 2000) and submicrometric voids (Pointer *et al.* 1988) have also been discussed as potential causes. We consider that the phenomenon cannot be explained by the high content of hydrous components alone. Detailed studies on hydrous species in crystalline and metamict zircon indicate that zircon rarely incorporates more than 1 wt.% of hydroxyl groups or H₂O molecules (Woodhead *et al.* 1991, Nasdala *et al.* 2001a), which is clearly insufficient to explain our low analytical totals. We found deficiencies up to 9 wt.% (Table 3), which would correspond to an elevated H₂O content exceeding 30 mol.%; this appears unlikely. On the other hand, samples described in the above papers addressing the question of hydrogen incorporation in zircon have not been affected by extensive secondary alteration processes, and may therefore not be directly comparable to our samples; this limits any conclusions by analogy. Consequently, micro-analyses of the samples for hydrogen in zircon showing deficient totals need to be done before this problem can be resolved.

Using the equation of Murakami *et al.* (1991), time-integrated α -doses were calculated for the zircon samples studied from present U and Th concentrations and assuming a self-irradiation period of ~300 million years. This value is based on the Hercynian age of emplacement of the batholith (Villaseca & Herreros 2000) and the assumption that samples have not experienced significant annealing since. Results suggest that most areas of the crystals yielding low analytical totals, which are rich in actinides (UO₂ + ThO₂ > 1 wt.%; Table 3), have experienced self-irradiation doses exceeding 8×10^{18} α -events per gram. Such high α -fluences are definitely sufficient to cause severe radiation-induced damage (Holland & Gottfried 1955, Murakami *et al.* 1991, Nasdala *et al.* 2001a). This was confirmed by Raman microprobe analyses: Raman band FWHM > 30 cm⁻¹ (Fig. 6) characterize these micro-areas as strongly radiation-damaged.

However, it is also not possible to simply relate the low totals to enhanced degrees of radiation damage.

There are many examples for strongly radiation-damaged, up to virtually amorphous, zircon samples that gave “normal” electron-microprobe totals of ~100 wt.% (Zhang *et al.* 2000, Nasdala *et al.* 2002). Nevertheless, these non-deficient samples of metamict zircon have extremely low Y, REE, Ca and Fe contents. On the contrary, most of the cases of metamict zircon from the SCS felsic granites are rich in U and Th, but also rich in trivalent cations (Y, HREE) and divalent cations (Ca, Fe, Mn). The increase in extent of cation substitutions in zircon is clearly related with the marked decrease of analytical totals: the greater the sum of ThO₂ + UO₂ (Fig. 10A), and oxides of trivalent and divalent cations, the lower the analytical total (Fig. 10B). The low analytical totals thus are obtained in areas of zircon crystals not only rich in actinides, which trigger metamictization, but also with a high abundance of heterovalent cations which, in some way, may enhance the disordered structure attained by the zircon, as suggested by Köppel & Sommerauer (1974). In this way, Rios *et al.* (2000) observed that high concentrations of point defects in radiation-damaged samples strongly affect the structural properties of crystalline zircon. Indeed, the abundance of these non-tetravalent cations that are not correlated with P substitution in the zircon structure would require also, to some degree, oxygen defects, which may contribute to the low analytical totals.

Zr/Hf values of zircon as a fractionation index of the magma

Heaman *et al.* (1990) considered that changes in zircon composition must be a function of changes in melt composition and degree of fractional crystallization. As a typical substitution is HfZr_{1-x}, the Zr:Hf ratio has been used either in matters of terminology (*e.g.*, Correia Neves *et al.* 1974) or as an index of magmatic differentiation (Černý *et al.* 1985). Many authors (Wark & Miller 1993, Irber *et al.* 1997, Wang *et al.* 2000) have pointed out that the concentration of Hf in zircon is variable, but depends mainly on the degree of evolution and the composition of the original granitic magma. The great variation in Zr/Hf values in zircon from subaluminous to peraluminous members of plutonic suites reveals a decoupling of Zr and Hf in the direction of enrichment in Hf with the degree of differentiation of the host granite (Linnen & Keppler 2002, Lowery *et al.* 2006).

In the diagram of Černý *et al.* (1985), the zircon displays an asymptotic curve (Fig. 11) in which both types of zircon are concentrated at intermediate values (70 – 25) in terms of Zr:Hf ratio. Type-1 zircon of granodiorites and monzogranites have Zr/Hf values from 110 to 25; in that of leucogranite, it varies from 80 to less than 10, and in crystals from aplite, the range is 40 – 30. The range of Zr:Hf in granodiorites and monzogranite of type-2 zircon is shorter and lower (63 – 31) than in type 1, and the opposite is observed for the

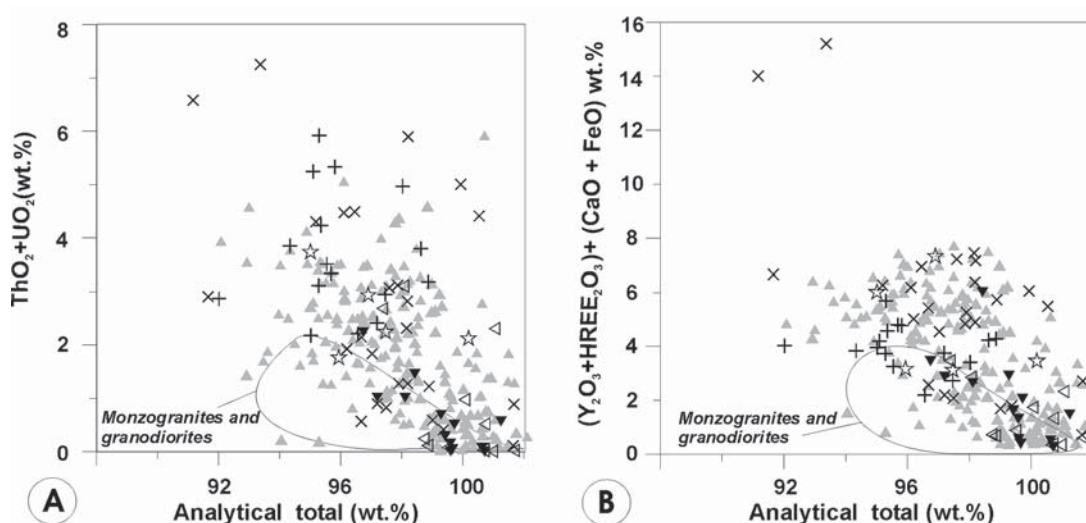


FIG. 10. A) Plot of (Th + U) versus (Y+HREE) for zircon of types-1 and 2 from all the plutons studied. B) Analytical total versus $(Y_2O_3 + HREE_2O_3) + (CaO + FeO)$ in wt.% in zircon crystals. See text for further explanations. Same symbols as in Figure 5.

more evolved granites ($53 < Zr/Hf < 3$ in leucogranites, and $71 < Zr/Hf < 14$ in aplites). Type-2 zircon from the La Pedriza leucogranite and La Cabrera pegmatites has the lowest Zr/Hf values (10 – 2.4) (Fig. 11). There are no significant differences in Zr/Hf between zircon of I- and S-type granites, as is also the case when comparing I- and A-type granites with a similar degree of differentiation (Wang *et al.* 2000).

We believe that the ratio Zr:Hf in zircon may be only a crude index of magmatic differentiation. As Zr in zircon is also replaced by other elements (*e.g.*, Y, HREE, Th and U) and as Hf may increase or decrease in a zoned single crystal of the same rock, the Zr:Hf ratio will display a large variation, even at the scale of a single crystal. For instance, in some grains of zircon from the La Pedriza leucogranite, Zr/Hf values decrease from 14 (core) to 2.4 (rim) (Table 3, no. 67263). In the Atalaya Real pluton, a single type-2 zircon crystal shows a similar range of Zr/Hf values (62 – 17) (Table 3, no. 96027) as the whole population of zircon crystals in the plutonic body. Furthermore, in a same thin section from the La Pedriza leucogranite (Table 3, no. 87165), type-2 zircon shows a Zr/Hf range of 49.4 to 4.6, as large as the variation found at the pluton scale.

Zircon composition and magma sources in the crust

In the compilation of zircon compositions made by Pupin (2000), the signature of zircon in the continental crust is marked by a Zr/Hf value in the range 36–45, which differs significantly from zircon in mantle-

derived rocks, with Zr/Hf around 60–68, or even higher if basic and undersaturated alkaline rocks are included (Pavlenko *et al.* 1957, Erlank *et al.* 1978). In Figure 12, we compare the previous Zr/Hf values collected in Figure 3 of Pupin (2000) with those from different peraluminous metamorphic rocks (migmatites, orthogneisses, granulite xenoliths) of central Spain (Villaseca *et al.* 2003) and those from the most primitive members of the S- and I-type granites studied. Following the criteria of Pupin (2000), we have excluded compositions from the rare-element-rich rim in fractionated granites. We obtain averaged Zr/Hf values of 46 for lower-crust granulite xenoliths, 49 for migmatites from the metasedimentary anatectic complex of Toledo, 39–45 for migmatites from SCS, and 56 for SCS augen orthogneisses. Consequently, purely crustal sources seem to have a slightly higher Zr/Hf ratio, in the range 36–56, rather than 36–45 as previously suggested (Pupin 2000).

The parental magmas of the plutonic suites studied have Zr/Hf values in the same range as that in zircon from crustal sources, and closely match those values of zircon crystals from the previously supposed restitic keel of the SCS batholith, the lower-crust granulite xenoliths (Villaseca *et al.* 1999). The chemical data on zircon are in accordance with previous geochemical and isotopic arguments for the minor participation of mantle-derived components in the genesis of the peraluminous SCS granitic rocks (Villaseca *et al.* 1998, 1999, Bea *et al.* 1999, Villaseca & Herreros 2000).

CONCLUSIONS

1. Two types of magmatic zircon crystals have been distinguished. The type-1 zircon appears mainly as isolated crystals in the least-evolved magmas. It exhibits oscillatory zoning in large idiomorphic crystals, and its composition is close to that of pure zircon, with increasing Hf, Th, U, Y and HREE contents from core to rim. The second type of zircon predominates in the most evolved magmas, as equant and smaller crystals, usually forming clusters with other accessory phases. Texturally, the crystals are mainly alveolar with micro-inclusions of other accessory minerals. Such type-2 zircon shows higher contents of Hf, Th, U, Y and HREE, with a decreasing trend of Th, U, Y, HREE and M^{2+} from core to rim, associated with an opposite Hf trend. Type-2 zircon is usually metamict and characterized by a low analytical total.

2. Mechanisms of substitution may be broadly correlated with the degree of magma differentiation. In the most felsic granites, the Zr site in zircon is preferentially occupied by (Th + U) rather than (Y + HREE). Divalent cations are also progressively introduced, and the total degree of substitution is high. Most zircon crystals show the dominant “xenotime” substitution, especially

zircon from S-type granites. Zircon crystals from some of the most evolved I-type granites show a high degree of (Th+U) incorporation.

3. Metamict zircon from the SCS granites shows a low analytical total, mostly in the range 91–98 wt.%. The deficiency of analytical totals correlates with the content of “non-formula” elements (especially the sum of M^{2+} and M^{3+} cations). The incorporation of H_2O in zircon is considered insufficient to explain such low analytical totals.

4. The composition of zircon is broadly correlated with that of their host granite composition. Nevertheless, the use of Zr:Hf ratio as an index of magma fractionation should be used with caution.

5. The most primitive granites studied have zircon Zr:Hf values with the same range as that of zircon from crustal sources (*e.g.*, residual granulites), supporting the hypothesis that the peraluminous SCS batholith was derived mainly from recycled crustal rock-types.

ACKNOWLEDGEMENTS

The authors thank Alfredo Fernández Larios for his assistance with the electron-microprobe analyses, and J.M. Caballero for providing microprobe data

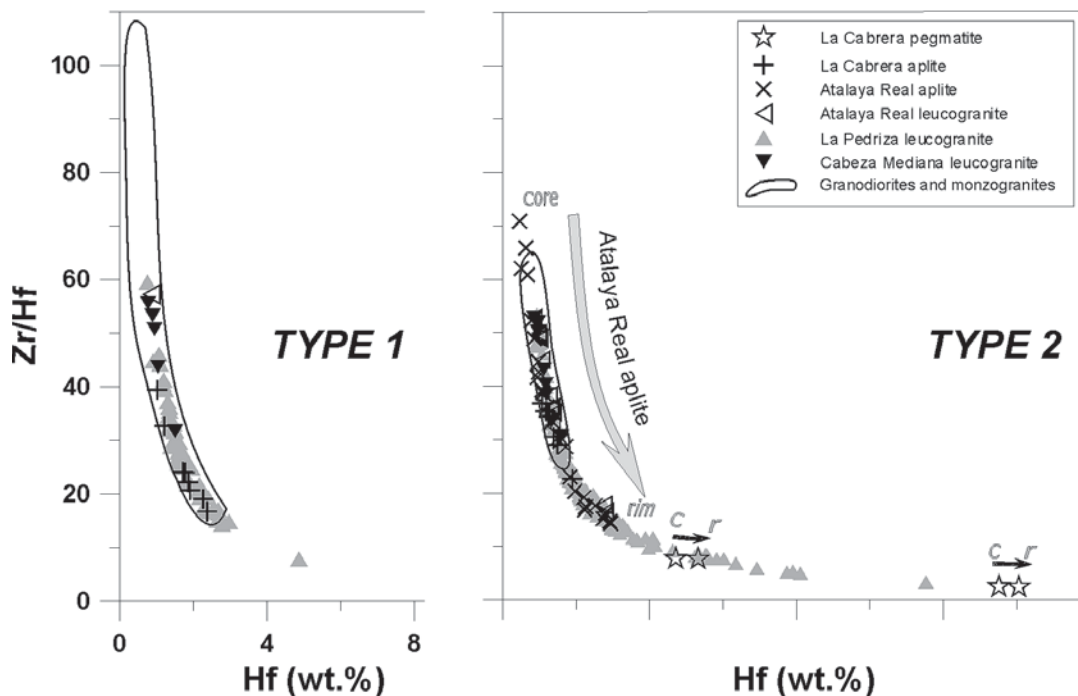


FIG. 11. The composition of zircon in terms of Hf (wt.%) versus Zr:Hf. In both diagrams, the enclosed area is the compositional field of zircon crystals in granodiorites and monzogranites. Compositional growth-zoning (core to rim) is also marked for some zircon crystals of type 2. Same symbols as in Figure 5.

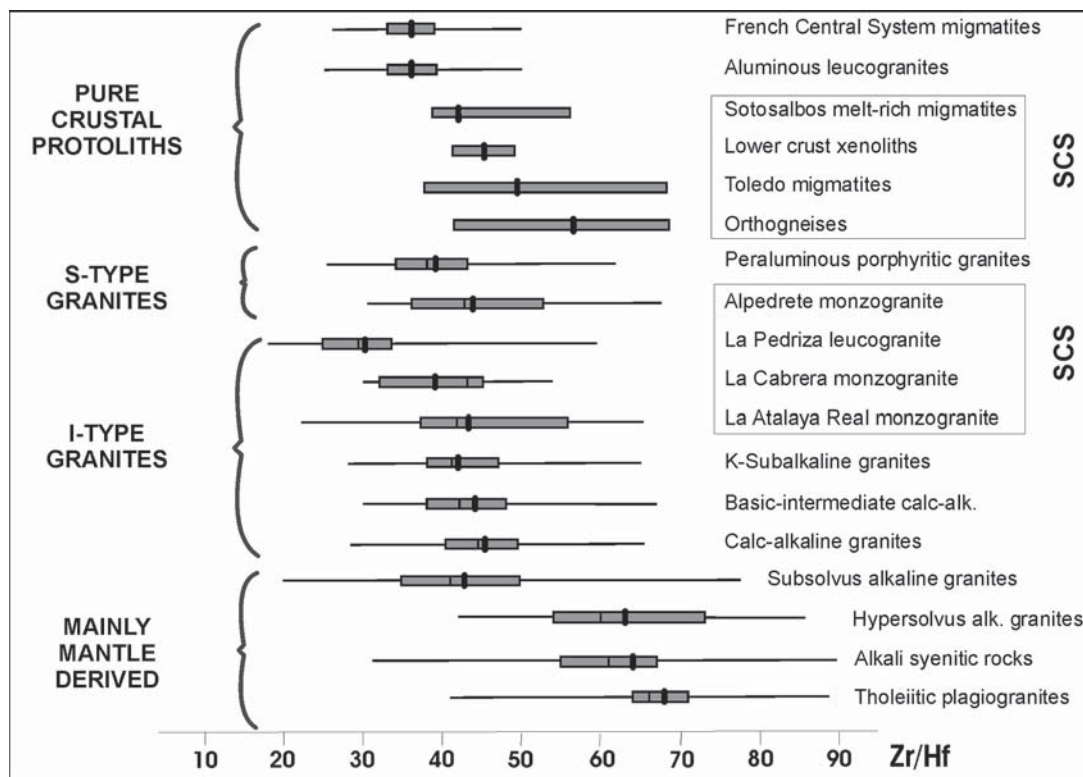


FIG. 12. Comparison of the Zr:Hf values in zircon of different crustal sources and types of granite. Box plots show the 25th and 75th percentiles (limits of the box), the median (thin line), the mean (coarse line) and the maximum and minimum values excluding outliers. Values for SCS rocks are taken from this study and from Villaseca *et al.* (2003); other values are taken from Pupin (2000).

for some samples from the La Pedriza pluton. We are indebted to John Cobbing for his detailed comments on a preliminary version of the manuscript, and to John M. Hanchar and an anonymous expert for most helpful reviews. Thanks are due to Robert Martin for editorial handling and his constructive suggestions. This work has been financially supported by the projects DGYCIT BTE2000-0575 and CGL2004-0575 of the Ministerio de Educación y Ciencia, Spanish Government.

REFERENCES

- AKHTAR, M.J., & WASSEM, S. (2001): Atomistic simulation studies of zircon. *Chem. Phys.* **274**, 109-120.
- BEA, F. (1996): Controls on the trace element composition of crustal melts. *Trans. R. Soc. Edinb.: Earth Sci.* **87**, 33-41.
- BEA, F., MONTERO, P. & MOLINA, J.F. (1999): Mafic precursors, peraluminous granitoids, and late lamprophyres in the Avila Batholith: a model for the generation of Variscan Batholiths in Iberia. *J. Geol.* **107**, 399-419.
- BELLIDO, F. (1979): *Estudio petrológico y geoquímico del plutón de La Cabrera*. Ph.D. thesis, Universidad Complutense de Madrid, Madrid, Spain.
- BELOUSOVA, E.A., GRIFFIN, W.L. & O'REILLY, S.Y. (2006): Zircon crystal morphology, trace element signatures and Hf isotope composition as a tool for petrogenetic modelling: examples from Eastern Australian granitoids. *J. Petrol.* **47**, 329-353.
- BELOUSOVA, E.A., WALTERS, S., GRIFFIN, W.L., O'REILLY, S.Y. & FISHER, N.I. (2002): Igneous zircon: trace-elements composition as indicator of source rock type. *Contrib. Mineral. Petrol.* **143**, 602-622.
- BREITER, K., FÖRSTER, H.-J. & ŠKODA, R. (2006): Extreme P-, Bi-, Nb-, Sc-, U- and F-rich zircon from fractionated perphosphorous granites: the peraluminous Podlesí granite system, Czech Republic. *Lithos* **88**, 15-34.
- CAIRONI, V., COLOMBO, A., TUNESI, A. & GRITTI, C. (2000): Chemical variations of zircon compared with morphological evolution during magmatic crystallization: an example

- from the Valle del Cervo pluton (Western Alps). *Eur. J. Mineral.* **12**, 779-794.
- ČERNÝ, P., MEINTZER, R.E. & ANDERSON, A.J. (1985): Extreme fractionation in rare-element granitic pegmatites: selected examples of data and mechanisms. *Can. Mineral.* **23**, 381-421.
- ČERNÝ, P. & SIIVOLA, J. (1980): The Tanco pegmatite at Bernic Lake, Manitoba. XII. Hafnian zircon. *Can. Mineral.* **18**, 313-321.
- CHERNIAK, D.J., HANCHAR, J.M. & WATSON, E.B. (1997): Rare-earth diffusion in zircon. *Chem. Geol.* **134**, 289-301.
- CORFU, F., HANCHAR, J.M., HOSKIN, P.W.O. & KINNY, P. (2003): Atlas of zircon textures. In *Zircon* (J.M. Hanchar & P.W.O. Hoskin, eds.). *Rev. Mineral. Geochem.* **53**, 469-500.
- CORREIA NEVES, J.M., LOPES NUNES, J.E. & SAHAMA, T.G. (1974): High hafnium members of the zircon-hafnon series from the granite pegmatites of Zambezia, Mozambique. *Contrib. Mineral. Petrol.* **48**, 73-80.
- ERLANK, A.J., SMITH, H.S., MARCHANT, J.W., CARDOSO, M.P. & AHRENS, L.H. (1978): Hafnium, In *Handbook of Geochemistry* (K.H. Wedepohl, ed.). Springer, Berlin, Germany (72D-E).
- EWING, R.C., MELDRUM, A., WANG, LUMIN, WEBER, W.J. & CORRALES, L.R. (2003): Radiation effects in zircon. In *Zircon* (J.M. Hanchar & P.W.O. Hoskin, eds.). *Rev. Mineral. Geochem.* **53**, 387-425.
- FEDO, C.M., SIRCOMBE, K.N. & RAINBIRD, R.H. (2003): Detrital zircon analysis of the sedimentary record. In *Zircon* (J.M. Hanchar & P.W.O. Hoskin, eds.). *Rev. Mineral. Geochem.* **53**, 277-303.
- FINCH, R.J., HANCHAR, J.M., HOSKIN, P.W.O. & PETERS, C.B. (2001): Rare-earth elements in synthetic zircon. 2. A single-crystal X-ray study of xenotime substitution. *Am. Mineral.* **86**, 681-689.
- FOWLER, A., PROKOPH, A., STERN, R. & DUPUIS, C. (2002): Organization of oscillatory zoning in zircon: analysis, scaling, geochemistry and model of a zircon from Kipawa, Quebec, Canada. *Geochim. Cosmochim. Acta* **66**, 311-328.
- GEISLER, T., PIDGEON, R.T., KURTZ, R., VAN BRONSWIJK, W. & SCHLEICHER, H. (2003a): Experimental hydrothermal alteration of partially metamict zircon. *Am. Mineral.* **88**, 1496-1513.
- GEISLER, T., RASHWAN, A.A., RAHN, M.K.W., POLLER, U., ZWINGMANN, H., PIDGEON, R.T., SCHLEICHER, H. & TOMASCHKE, F. (2003b): Low-temperature hydrothermal alteration of natural metamict zircon from the Eastern Desert, Egypt. *Mineral. Mag.* **67**, 485-508.
- GEISLER, T. & SCHLEICHER, H. (2000): Improved U – Th – total Pb dating of zircons by electron microprobe using a new background modelling procedure and Ca as a chemical criterion of fluid-induced U–Th–Pb discordance in zircon. *Chem. Geol.* **163**, 269-285.
- HANCHAR, J.M., FINCH, R.J., HOSKIN, P.W.O., WATSON, E.B., CHERNIAK, D.J. & MARIANO, A.N. (2001): Rare earth elements in synthetic zircon. 1. Synthesis, and rare earth element and phosphorus doping. *Am. Mineral.* **86**, 667-680.
- HANCHAR, J.M. & HOSKIN, P.W.O. (2003): Zircon. *Rev. Mineral. Geochem.* **53**.
- HANCHAR, J.M. & MILLER, C.F. (1993): Zircon zonation patterns as revealed by cathodoluminescence and backscattered electron images: implications for interpretation of complex crustal histories. *Chem. Geol.* **110**, 1-13.
- HANCHAR, J.M. & WATSON, E.B. (2003): Zircon saturation thermometry. In *Zircon* (J.M. Hanchar & P.W.O. Hoskin, eds.). *Rev. Mineral. Geochem.* **53**, 89-112.
- HARRISON, T.M. & WATSON, E.B. (1983): Kinetics of dissolution and zirconium diffusion in granitic melts of variable water content. *Contrib. Mineral. Petrol.* **84**, 66-72.
- HEAMAN, L.M., BOWINS, R. & CROCKET, J. (1990): The chemical composition of igneous zircon suites: implications for geochemical tracer studies. *Geochim. Cosmochim. Acta* **54**, 1597-1607.
- HIGGINS, M.D. (1994): Numerical modelling of crystal shapes in thin sections: estimation of crystal habit and true size. *Am. Mineral.* **79**, 113-119.
- HOLLAND, H.D. & GOTTFRIED, D. (1955): The effect of nuclear radiation on the structure of zircon. *Acta Crystallogr.* **8**, 291-300.
- HOSKIN, P.W.O. (2000): Patterns of chaos: fractal statistics and the oscillatory chemistry of zircon. *Geochim. Cosmochim. Acta* **64**, 1905-1923.
- HOSKIN, P.W.O. & IRELAND, T.R. (2000): Rare earth element chemistry of zircon and its use as a provenance indicator. *Geology* **28**, 627-630.
- HOSKIN, P.W.O., KINNY, P.D., WYBORN, D. & CHAPPELL, B.W. (2000): Identifying accessory mineral saturation during differentiation in granitoid magmas: an integrated approach. *J. Petrol.* **41**, 1365-1396.
- HOSKIN, P.W.O. & SCHALTEGGER, U. (2003): The composition of zircon and igneous and metamorphic petrogenesis. In *Zircon* (J.M. Hanchar & P.W.O. Hoskin, eds.). *Rev. Mineral. Geochem.* **53**, 27-62.
- IRBER, W., FÖRSTER, H.-J., HECHT, L., MÖLLER, P. & MORTEANI, G. (1997): Experimental, geochemical, mineralogical and O-isotope constraints on the late-magmatic history of the Fichtelgebirge granites (Germany). *Geol. Rundsch.* **86**, Suppl., S110-S124.

- JACKSON, S.E., PEARSON, N.J., GRIFFIN, W.L. & BELOUSOVA, E.A. (2004): The application of laser ablation – inductively coupled plasma – mass spectrometry to *in situ* U–Pb zircon geochronology. *Chem. Geol.* **211**, 47–69.
- JAROSEWICH, E. & BOATNER, L.A. (1991): Rare-earth element reference samples for electron microprobe analysis. *Geostand. Newslett.* **15**, 397–399.
- JAROSEWICH, E., NELEN, J.A. & NORBERG, J.A. (1980): Reference samples for electron microprobe analysis. *Geostand. Newslett.* **4**, 43–47.
- KEMPE, U., GRUNER, T., NASDALA, L. & WOLF, D. (2000): Relevance of cathodoluminescence for the interpretation of U–Pb zircon ages, with an example of an application to a study of zircons from the Saxonian Granulite Complex, Germany. In *Cathodoluminescence in Geosciences* (M. Pagel, V. Barbin, P. Blanc & D. Ohnenstetter, eds.). Springer-Verlag, Berlin, Germany (415–455).
- KEMPE, U., GRUNER, T., RENNO, A.D., WOLF, D. & RENÉ, M. (2004): Discussion on Wang *et al.* (2000): Chemistry of Hf-rich zircons from the Laoshan I- and A-type granites, eastern China. *Mineral. Mag.* **68**, 669–675.
- KÖPPEL, V. & SOMMERAUER, J. (1974): Trace elements and the behaviour of the U–Pb system in inherited and newly formed crystals. *Contrib. Mineral. Petrol.* **43**, 71–82.
- KRETZ, R. (1983): Symbols for rock-forming minerals. *Am. Mineral.* **68**, 277–279.
- LINNEN, R.L. & KEPPLER, H. (2002): Melt composition control of Zr/Hf fractionation in magmatic processes. *Geochim. Cosmochim. Acta* **66**, 3293–3301.
- LOWERY, L.E., MILLER, C.F., WOODEN, J.L., MAZDAB, F.K. & BEA, F. (2006): Hf and Ti zoning in zircon: detailed records of magmatic processes. *Geophys. Res. Abstr.* **8**, 01258.
- LUMPKIN, G.R. & CHAKOUMAKOS, B.C. (1988): Chemistry and radiation effects of thorite-group minerals from the Harding pegmatite, Taos County, New Mexico. *Am. Mineral.* **73**, 1405–1419.
- MATHIEU, R., ZETTERSTRÖM, L., CUNEY, M., GAUTHIER-LAFAYE, F. & HIDAKA, H. (2001): Alteration of monazite and zircon and lead migration as geochemical tracers of fluid paleocirculation around the Oklo–Okélobondo and Bangombé natural nuclear reaction zones (Franceville Basin, Gabon). *Chem. Geol.* **171**, 147–171.
- MEZGER, K. & KRÖGSTAD, E.J. (1997): Interpretation of discordant U–Pb ages: an evaluation. *J. Metam. Geol.* **15**, 127–140.
- MURAKAMI, T., CHAKOUMAKOS, B.C., EWING, R.C., LUMPKIN, G.R. & WEBER, W.J. (1991): Alpha-decay event damage in zircon. *Am. Mineral.* **76**, 1510–1532.
- NASDALA, L., BERAN, A., LIBOWITZKY, E. & WOLF, D. (2001a): The incorporation of hydroxyl groups and molecular water in natural zircon (ZrSiO₄). *Am. J. Sci.* **301**, 831–857.
- NASDALA, L. & HANCHAR, J.M. (2005): Comment on: Application of Raman spectroscopy to distinguish metamorphic and igneous zircon (Xian *et al.*, *Anal. Lett.* 2004, v. 37, p. 119). *Anal. Lett.* **38**, 727–734.
- NASDALA, L., IRMER, G. & WOLF, D. (1995): The degree of metamictization in zircons: a Raman spectroscopic study. *Eur. J. Mineral.* **7**, 471–478.
- NASDALA, L., LENGAUER, C.L., HANCHAR, J.M., KRONZ, A., WIRTH, R., BLANC, P., KENNEDY, A.K. & SEYDOUX-GUILLAUME, A.-M. (2002): Annealing radiation damage and the recovery of cathodoluminescence. *Chem. Geol.* **191**, 121–140.
- NASDALA, L., WENZEL, M., VAVRA, G., IRMER, G., WENZEL, T. & KOBER, B. (2001b): Metamictisation of natural zircon: accumulation versus thermal annealing of radioactivity-induced damage. *Contrib. Mineral. Petrol.* **141**, 125–144.
- PARRISH, R.R. & NOBLE, S.R. (2003): Zircon U–Th–Pb geochronology by isotope dilution – thermal ionisation mass spectrometry (ID–TIMS). In *Zircon* (J.M. Hanchar & P.W.O. Hoskin, eds.). *Rev. Mineral. Geochem.* **53**, 183–213.
- PAVLENKO, A.S., VAINSHTEIN, E.E. & SHEVALEEVSKII, I.D. (1957): On the hafnium–zirconium ratio in igneous and metasomatic rocks. *Geochemistry*, 411–431.
- PÉREZ-SOBA, C. (1992): *Petrología y geoquímica del macizo granítico de La Pedriza, Sistema Central Español*. Ph.D. thesis, Universidad Complutense de Madrid, Madrid, Spain.
- PETERMAN, Z.E., ZARTMAN, R.E. & SIMS, P.K. (1986): A protracted Archean history in the Watersmeet gneiss dome, northern Michigan. *U.S. Geol. Surv. Bull.* **1622**, 51–64.
- PIDGEON, R.T., NEMCHIN, A.A. & HITCHEN, G.J. (1998): Internal structures of zircon from Archean granites from the Darling Range batholith: implications for zircon stability and the interpretation of zircon U–Pb ages. *Contrib. Mineral. Petrol.* **132**, 288–299.
- POINTER, C.M., ASHWORTH, J.R. & IXER, R.A. (1988): The zircon–thorite mineral group in metasomatized granite, Ririwai, Nigeria. 2. Zoning, alteration and exsolution in zircon. *Mineral. Petrol.* **39**, 21–37.
- PUPIN, J.P. (1980): Zircon and granite petrology. *Contrib. Mineral. Petrol.* **73**, 207–220.
- PUPIN, J.P. (2000): Granite genesis related to geodynamics from Hf–Y in zircon. *Trans. R. Soc. Edinb.: Earth Sci.* **91**, 245–256.
- RÍOS, S., MALCHEREK, T., SALJE, E.K.H. & DOMENEGHETTI, C. (2000): Localized defects in radiation-damaged zircon. *Acta Crystallogr.* **B56**, 947–952.
- ROMANS, P.A., BROWN, L.L. & WHITE, J.C. (1975): An electron microprobe study of yttrium, rare earth, and

- phosphorus distribution in zoned and ordinary zircon. *Am. Mineral.* **60**, 475-480.
- RUBATTO, D., WILLIAMS, I.S. & BUICK, I.S. (2001): Zircon and monazite response to prograde metamorphism in the Reynolds Range, central Australia. *Contrib. Mineral. Petrol.* **140**, 458-468.
- RUBIN, J.N., HENRY, C.D. & PRICE, J.G. (1989): Hydrothermal zircon overgrowths, Sierra Blanca Peaks, Texas. *Am. Mineral.* **74**, 865-869.
- SEIDLER, K., LENTZ, D.R., HALL, D.C. & SUSAK, N. (2005): Zircon-rich Ta-Nb-REE mineralization in the radioactive McKeel Lake pegmatite-aplite system, Welsford Igneous Complex, southwestern New Brunswick. *Explor. Mining Geol.* **14**, 79-94.
- SMITH, D.G.W., DE ST. JORRE, L., REED, S.J.B. & LONG, J.V.P. (1991): Zonally metamictized and other zircon from Thor Lake, Northwest Territories. *Can. Mineral.* **29**, 301-309.
- SOLAR, G.S., PRESSLEY, R.A., BROWN, M. & TUCKER, R.D. (1998): Granite ascent in convergent orogenic belts: testing a model. *Geology* **26**, 711-714.
- SPEER, J.A. (1980): Zircon. In Orthosilicates (P.H. Ribbe, ed.). *Rev. Mineral.* **5**, 67-112.
- UHER, P., BREITER, K., KLEKA, M. & PIVEC, E. (1998): Zircon in highly evolved Hercynian Homolka granite, Moldanubian zone, Czech Republic: indicator of magma source and petrogenesis. *Geol. Carpathica* **49**, 151-160.
- UHER, P. & ČERNÝ, P. (1998): Zircon in Hercynian granitic pegmatites of the western Carpathians, Slovakia. *Geol. Carpathica* **49**, 261-270.
- VALLEY, J.W. (2003): Oxygen isotopes in zircon. In Zircon (J.M. Hancher & P.W.O. Hoskin, eds.). *Rev. Mineral. Geochem.* **53**, 343-385.
- VAVRA, G. (1994): Systematics of internal zircon morphology in major Variscan granitoid types. *Contrib. Mineral. Petrol.* **117**, 331-344.
- VILLASECA, C., BARBERO, L. & ROGERS, G. (1998): Crustal origin of Hercynian peraluminous granitic batholiths of central Spain: petrological, geochemical and isotopic (Sr, Nd) constraints. *Lithos* **43**, 55-79.
- VILLASECA, C., DOWNES, H., PIN, C. & BARBERO, L. (1999): Nature and composition of the lower continental crust in central Spain and the granulite-granite linkage: inferences from granulitic xenoliths. *J. Petrol.* **40**, 1465-1496.
- VILLASECA, C., EUGERCIOS, L., SNELLING, N., HUERTAS, M.J. & CASTELLÓN, T. (1995): Nuevos datos geocronológicos (Rb-Sr, K-Ar) de granitoides hercínicos de la Sierra de Guadarrama. *Rev. Soc. Geol. España* **8**, 137-148.
- VILLASECA, C. & HERREROS, V. (2000): A sustained felsic magmatic system: the Hercynian granitic batholith of the Spanish Central System. *Trans. R. Soc. Edinb.: Earth Sci.* **91**, 207-219.
- VILLASECA, C., MARTÍN ROMERA, C., DE LA ROSA, J. & BARBERO, L. (2003): Residence and redistribution of REE, Y, Zr, Th and U during granulite-facies metamorphism: behaviour of accessory and major phases in peraluminous granulites of central Spain. *Chem. Geol.* **200**, 293-323.
- WANG, RU-CHENG, FONTAN, F., XU, SHI JIN, CHEN, XIAO MING & MONCHOUX, P. (1996): Hafnian zircon from the apical part of the Suzhou granite, China. *Can. Mineral.* **34**, 1001-1010.
- WANG, RU-CHENG, ZHAO, G.T., LU, J.J., CHEN, X.M., XU, S.J. & WANG, D.Z. (2000): Chemistry of Hf-rich zircon from the Laoshan I- and A-type granites, eastern China. *Mineral. Mag.* **64**, 867-877.
- WARK, D.A. & MILLER, C.F. (1993): Accessory mineral behaviour during differentiation of a granite suite: monazite, xenotime and zircon in the Sweetwater Wash pluton, southeastern California, U.S.A. *Chem. Geol.* **110**, 49-67.
- WATSON, E.B. (1996): Dissolution, growth and survival of zircons during crustal fusion: kinetic principles, geologic models and implications for isotopic inheritance. *Trans. R. Soc. Edinb.: Earth Sci.* **87**, 43-56.
- WATSON, E.B., WARK, D.A. & THOMAS, J.B. (2006): Crystallization thermometers for zircon and rutile. *Contrib. Mineral. Petrol.* **151**, 413-433.
- WOODHEAD, J.A., ROSSMAN, G.R. & THOMAS, A.P. (1991): Hydrous species in zircon. *Am. Mineral.* **76**, 1533-1546.
- ZHANG, M. & SALJE, E.K.H. (2001): Infrared spectroscopic analysis of zircon: radiation damage and the metamict state. *J. Phys. Condens. Matter* **13**, 3057-3071.
- ZHANG, M., SALJE, E.K.H. & EWING, R.C. (2003): Oxidation state of uranium in metamict and annealed zircon: near-infrared spectroscopic quantitative analysis. *J. Phys. Condens. Matter* **15**, 3445-3470.
- ZHANG, M., SALJE, E.K.H., FARNAN, I., GRAEME-BARBER, A., DANIEL, P., EWING, R.C., CLARK, A.M. & LEROUX, H. (2000): Metamictization of zircon: Raman spectroscopic study. *J. Phys. Condens. Matter* **12**, 1915-1925.

Received March 18, 2005, revised manuscript accepted September 27, 2006.